

Cite this: *RSC Sustainability*, 2024, 2, 2239

# Ionic-liquid-processed keratin-based biocomposite films with cellulose and chitin for sustainable dye removal†

Cariny Polesca,<sup>ab</sup> Helena Passos,<sup>id</sup> Pedro Y. S. Nakasu,<sup>b</sup> João A. P. Coutinho,<sup>id</sup> Mara G. Freire<sup>id</sup>\*<sup>a</sup> and Jason P. Hallett<sup>id</sup>\*<sup>b</sup>

Poultry is a widely consumed meat worldwide; however, its industrial processing generates a significant amount of feather waste. Since the major component of chicken feathers is keratin (90 wt%), this study focused on using acetate-based ionic liquids (ILs) to fully dissolve chicken feathers and recover keratin, using a sustainable and cost-effective approach, ultimately allowing waste valorisation. The recovered keratin was processed into films, either pure or blended with cellulose and  $\alpha$ -chitin, aiming to develop a structural polymer biocomposite with improved mechanical properties. Experimental parameters were evaluated using different blend ratios, altering the pH, and adding glycerol as a plasticiser. Physico-chemical analysis revealed that all films exhibited hydrophilic behaviour and are stable up to 160 °C. Furthermore, the tensile strength of the keratin-based films significantly increased by adding chitin (achieving up to 66 MPa). Considering the growing significance of biopolymer-based films in wastewater treatment applications, the keratin-based films were evaluated as adsorbents for dye removal. Reactive Blue 4 (RB4) was used as a model dye, and the adsorption kinetics and isotherms were investigated. Between the studied films, the maximum adsorption capacity (55.7 mg g<sup>-1</sup>) was obtained for the keratin film, emphasising the potential of this biomaterial in wastewater treatment.

Received 17th April 2024  
Accepted 30th June 2024

DOI: 10.1039/d4su00179f

rsc.li/rscsus

## Sustainability spotlight

This article presents a novel approach to the smart design of circular biocomposites by combining low-cost and abundant biopolymers, producing keratin-based films either pure or blended with cellulose and  $\alpha$ -chitin, each of which is derived from waste. A bio-based solvent was used for biopolymer dissolution, enabling a sustainable and cost-effective approach. As an exemplar application, the films were used as adsorbents for contaminated water, achieving higher adsorption capacity than common adsorbents reported in the literature. This marks the first reported results on developing keratin–chitin films, offering a more sustainable alternative to chitosan. This work aligns with the UN Sustainable Development Goals: decent work, economic growth (SDG 8), and responsible consumption and production (SDG 12).

## Introduction

The global meat industry produces around 15 million tons of chicken feather waste annually,<sup>1</sup> posing challenges such as negative impacts on the land composition and environmental pollution (affecting nitrogen and phosphorus cycles), and

a high cost for disposal.<sup>2</sup> Chicken feathers contain nearly 90 wt% keratin, a valuable protein source for sustainable and environmentally friendly resource development.<sup>1,3</sup> However, keratin recovery is challenging, mainly because of the inter- and intramolecular disulphide bonds between sulphur-containing amino acid residues and extensive cross-linking, which are resistant to water, weak acids, and organic solvents.<sup>2,4,5</sup> Ionic liquids (ILs) have been investigated to overcome such issues due to their excellent dissolution capability and high efficiency for protein recovery.<sup>6–11</sup> ILs are salts formed by a large organic cation and an organic or inorganic anion, with lower melting temperatures than inorganic salts.<sup>5,8,12</sup> Recently, we demonstrated the ability of acetate-based ILs for feather dissolution, which is due to the anion's high hydrogen-bonding acceptor ability, further providing an efficient keratin recovery (up to 93 wt%) and a more sustainable pathway for producing keratin films.<sup>11,13</sup> The IL recovery (over at least four cycles) was

<sup>a</sup>CICECO – Aveiro Institute of Materials, Department of Chemistry, University of Aveiro, 3810-193 Aveiro, Portugal. E-mail: maragfreire@ua.pt

<sup>b</sup>Department of Chemical Engineering, Imperial College London, South Kensington Campus, London SW7 2AZ, UK. E-mail: j.hallett@imperial.ac.uk

<sup>c</sup>LSRE-LCM – Laboratory of Separation and Reaction Engineering – Laboratory of Catalysis and Materials, Faculty of Engineering, University of Porto, 4200-465 Porto, Portugal

<sup>d</sup>ALICE – Associate Laboratory in Chemical Engineering, Faculty of Engineering, University of Porto, 4200-465 Porto, Portugal

† Electronic supplementary information (ESI) available. See DOI: <https://doi.org/10.1039/d4su00179f>



successfully achieved, and a techno-economic assessment of the process was performed, demonstrating the potential for a cost-effective and environmentally friendly process.<sup>13</sup>

Keratin applications involve several areas, including use in the biomedical field and as an adsorbent for water treatment/remediation.<sup>14–16</sup> Water contamination is a global concern, with the textile industry generating more than 7 million tons of toxic, carcinogenic, and nonbiodegradable dyes annually.<sup>15</sup> These substances pose threats to human health and aquatic life.<sup>3,16</sup> In the textile industry, reactive dyes (e.g. reactive blue 4, RB4) are widely used (around 700 000 tons of dyes are annually produced) and present acute toxicity (LD<sub>50</sub> oral 8.98 mg kg<sup>-1</sup>).<sup>17,18</sup> The environmental impact of RB4 assessed by EPI Suite™ confirms its slow environmental degradation (150 days in water and soil and 600 days in sediment),<sup>19</sup> highlighting the urgency to develop strategies to mitigate this concern.

Several water treatment methods have been investigated to address this issue, including chemical oxidation, electrochemical oxidation, ion exchange, and adsorption.<sup>14</sup> The typical water treatment technologies are energy-intensive and involve unsustainable synthetic materials. However, adsorption, particularly using biomaterials like keratin,<sup>20–22</sup> has shown promising results as a clean and effective alternative method.<sup>3</sup> Keratin-based adsorbents are attractive because their functional groups (e.g. hydrophobic and hydrophilic amino acids and carboxyl groups, such as -NH<sub>2</sub>, -COOH, -SH, and -OH) act as effective adsorption sites to a broad range of aqueous contaminants, accentuating their performance. Keratin is a fibrous protein with a high surface area, enhancing its adsorption capacity.<sup>14,23,24</sup> Moreover, it is an available, biodegradable, non-toxic, low-cost biomaterial.<sup>3,15,21</sup> While previous studies have demonstrated the feasibility of keratin-based adsorbents,<sup>25,26</sup> challenges remain in cost-effectiveness processes for its recovery and poor tensile strength of the produced films.<sup>27</sup> To overcome some of these challenges, we propose the use of the previously developed cost-effective process for keratin recovery using ILs,<sup>11,13</sup> focusing now on preparing keratin-based films with improved mechanical properties by creating blends with cellulose and chitin for water purification. The idea is to employ the smart design of biocomposites by combining different types of low-cost and relatively abundant biopolymers. To blend with keratin, two structural biopolymers were chosen to enhance the mechanical properties of the films without compromising their biodegradability:<sup>24,28</sup> cellulose—an abundant biopolymer with good mechanical and thermal properties<sup>29,30</sup>—and chitin—an acetylated polysaccharide with outstanding mechanical properties, such as high strength and high toughness.<sup>31,32</sup> The strong interaction between keratin and these polymers is attributed to their strong hydrogen bonding network between their functional groups (CH<sub>3</sub>, CONH, NH<sub>2</sub> and OH).<sup>33</sup>

The processing conditions for the preparation of keratin films (e.g. keratin concentration, pH, addition of glycerol as a plasticiser, effect of three acetate-based ILs, and the biopolymer ratio) were varied by means of the design of experiments to evaluate their influence on the film properties. All keratin-based films were characterised using physicochemical, mechanical, and morphological analyses, and their potential as

adsorbent materials for dye removal was explored using RB4. The adsorption kinetics and isotherms were examined. In summary, this work focuses on developing keratin-based films with adequate properties for application in wastewater treatment, while contributing to waste valorisation.

## Materials and methods

### Materials

Chicken feathers were collected from Campoaves Company in Oliveira de Frades, Portugal, and pre-treated before dissolution, as reported in the literature.<sup>11</sup> The ILs used, *viz.* 1-butyl-3-methylimidazolium acetate ([C<sub>4</sub>C<sub>1</sub>im][C<sub>1</sub>CO<sub>2</sub>]) (>95 wt% pure) and 1-ethyl-3-methylimidazolium acetate [C<sub>2</sub>C<sub>1</sub>im][C<sub>1</sub>CO<sub>2</sub>] (>95 wt% pure) were purchased from Sigma-Aldrich. Ethanol (99.8 wt% pure), acetic acid (>99.7 wt% pure), sodium hydroxide (NaOH), and ethylene glycol were acquired from Fisher Scientific. Glycerol (>99 wt% pure) was purchased from Acros Organics. Cholinium bicarbonate, cellulose highly purified, hydrochloric acid (HCl) (>37 wt% pure) and RB4 (35 wt% pure) were obtained from Sigma-Aldrich.  $\alpha$ -Chitin from shrimp was purchased from Apollo Scientific. Cholinium acetate ([N<sub>111(2OH)</sub>][C<sub>1</sub>CO<sub>2</sub>]) was synthesised as previously described by Muhammad *et al.*<sup>34</sup> Briefly, acetic acid was added dropwise to cold cholinium bicarbonate in a round-bottom flask and stirred overnight. The moisture content in the synthesised IL was removed using a rotatory evaporator consisting of Rotavapor R-10, heating bath B-491, vacuum pump V-700 and vacuum controller V-850 (all from Buchi, Switzerland). The water content was determined using a V20 Volumetric Karl-Fischer titrator (Mettler Toledo). The purity of the IL, confirmed by proton nuclear magnetic resonance (<sup>1</sup>H-NMR), is available in the ESI (Fig. S1).††

### Chicken feather dissolution and keratin recovery

Chicken feathers were dissolved, as previously reported by our research group.<sup>11,13</sup> Different aqueous solutions of [C<sub>4</sub>C<sub>1</sub>im][C<sub>1</sub>CO<sub>2</sub>], [C<sub>2</sub>C<sub>1</sub>im][C<sub>1</sub>CO<sub>2</sub>], and [N<sub>111(2OH)</sub>][C<sub>1</sub>CO<sub>2</sub>] (80 wt% IL + 20 wt% water) were used for feather dissolution at 100 °C for 4 h in a solid : liquid (chicken feather : solvent) ratio of 1 : 20 w/w. After dissolution, keratin was recovered by adding water as a coagulant solvent in a solution : coagulant ratio of 1 : 2 w/w at 5 °C for 1 h. Then, the solution was centrifuged for 20 min at 4000 rpm in a refrigerator centrifuge machine (VWR® Mega Star 4.0), promoting the separation of the precipitated keratin. The protein was then washed with DI water to remove any residual IL and centrifuged under the previously described conditions. The wet keratin was used for film processing. Keratin recovery yield of up to 93 wt% was obtained, in agreement with previous assays.<sup>11,13</sup>

### Keratin-based film processing

Wet keratin recovered by [C<sub>4</sub>C<sub>1</sub>im][C<sub>1</sub>CO<sub>2</sub>] was used to investigate the film processing conditions: protein concentration (on

† NMR spectra of [N<sub>111(2OH)</sub>][C<sub>1</sub>CO<sub>2</sub>], speciation of the RB4 dye according to pH changes and physicochemical properties of keratin-based films.



**(i) Biopolymer dissolution****(ii) Bio-based film processing**

Fig. 1 Schematic representation of the biopolymer dissolution (i) and the keratin-based film processing (ii) proposed in this work.

Table 1 Sample names and conditions used for preparing keratin-based films<sup>a</sup>

Sample	IL	Biopolymer (wt%)	pH	Glycerol (wt%)
KER-5	[C <sub>4</sub> C <sub>1</sub> im][C <sub>1</sub> CO <sub>2</sub> ]	5	6.4	—
KER-15		15		
KER-20		20		
KER-pH9		15	9.0	—
KER-pH12		15	12.0	—
KER-gly5		15	6.4	5
KER-gly10		15		10
KER-C2	[C <sub>2</sub> C <sub>1</sub> im][C <sub>1</sub> CO <sub>2</sub> ]	15	6.4	—
KER-N <sub>111</sub>	[N <sub>111(2OH)</sub> ][C <sub>1</sub> CO <sub>2</sub> ]	15		
KER-CELL-C2 75 : 25	[C <sub>2</sub> C <sub>1</sub> im][C <sub>1</sub> CO <sub>2</sub> ]	15*	6.4	10
KER-CELL-C2 50 : 50		15**		
KER-CHI-C2 75 : 25		15*		
KER-CHI-C2 50 : 50		15**		
KER-CELL-N <sub>111</sub> 75 : 25	[N <sub>111(2OH)</sub> ][C <sub>1</sub> CO <sub>2</sub> ]	15*	6.4	10
KER-CELL-N <sub>111</sub> 50 : 50		15**		
KER-CHI-N <sub>111</sub> 75 : 25		15*		
KER-CHI-N <sub>111</sub> 50 : 50		15**		

<sup>a</sup> \* = 75 wt% keratin + 25 wt% cellulose or chitin; \*\* = 50 wt% keratin + 50 wt% cellulose or chitin.

distilled water), solution pH (adjusted with NaOH 1 M), and addition of glycerol as a plasticiser. The mixture was mixed under constant magnetic stirring at 60 °C for 1 h. The solution was cast on a silicone moulding and placed in an air oven at 50 °C for 24 h. A control keratin solution (KER-15; 15 wt% keratin, without glycerol and pH modification) was used to prepare films using keratin recovered by [C<sub>2</sub>C<sub>1</sub>im][C<sub>1</sub>CO<sub>2</sub>] and [N<sub>111(2OH)</sub>][C<sub>1</sub>CO<sub>2</sub>], aiming to investigate the IL influence on the keratin film properties. Then, keratin–cellulose and keratin–chitin biocomposite films were processed, aiming to understand the

impact of the blend composition on the film properties. Keratin–cellulose (75 : 25 and 50 : 50 w/w) and keratin–chitin (75 : 25 and 50 : 50 w/w) films were processed by adding keratin and cellulose or chitin in distilled water (15 wt% of biopolymers). The film processing followed the previously described procedure for pure keratin films. The keratin-based film processing is schematically summarized in Fig. 1, and the conditions used for the processing and their sample names are presented in Table 1.



### Characterisation of keratin-based films

The Fourier transform infrared attenuated total reflectance (FTIR-ATR) spectra of the films processed under different conditions were acquired by FTIR spectroscopy (Spectrum One FTIR system, PerkinElmer, Wellesley, MA). The functional groups available on films were analysed at room temperature, in a frequency range of 4000–400  $\text{cm}^{-1}$ , by accumulating 16 scans, with a resolution of 4  $\text{cm}^{-1}$ , and an interval of 1  $\text{cm}^{-1}$ .

Thermogravimetric analysis (TGA) was carried out on a TA Q500 (TA Instruments, USA) TGA analyser. Keratin-based films were placed in an aluminium pan and further analysed under a nitrogen gas at a flow rate of 25  $\text{mL min}^{-1}$ . The samples were heated at a rate of 20  $^{\circ}\text{C min}^{-1}$  in the temperature range from 30 to 600  $^{\circ}\text{C}$ .

To investigate the hydrophilicity of the films, the contact angle was determined using a semi-automatic wettability analysis with high dosing precision (DSA25S, Krüss). Adding a drop of 7  $\mu\text{L}$  of ethylene glycol at a rate of 7  $\mu\text{L s}^{-1}$ , multiple measurements were made on keratin-based films. Further details on the procedure can be found elsewhere.<sup>11</sup>

Using a Lloyd EZ 50 testing machine, the tensile strength of the films was determined. Keratin-based films were cut into rectangular shapes (4  $\text{cm} \times 1 \text{ cm}$ ), and three replicates were carried out. The tensile strength (MPa) was calculated by dividing the obtained value (N) by the cross-sectional area of the films.

Scanning electron microscopy (SEM) was performed using a high-resolution field-emission Zeiss Auriga Cross Beam. Aiming to ensure the conductivity of the films, they were coated with chromium (15 nm) in a Q150 TS machine before the sample analysis. Images were obtained using an accelerating voltage of 5 kV and a working distance of 5 nm.

### Adsorption properties of keratin-based films

The adsorption of RB4 was addressed using keratin-based films with the best achieved properties (high thermal degradation and high tensile strength). First, the adsorption kinetics was investigated using 10 mL of RB4 solution (60 ppm) at pH 2.0 with 5 mg of adsorbent for 0–360 min. The effect of pH on adsorption performance was studied in a pH range of 2.0–8.0 using 10 mL of RB4 solution (60 ppm) with 5 mg of adsorbent for 300 min. Then, the effect of the initial concentration of RB4 (10–60 ppm) was investigated for all keratin-based films using 5 mg of adsorbent and 10 mL of RB4 solution at pH 2.0 for 300 min. The samples were maintained by stirring (150 rpm) at 30  $^{\circ}\text{C}$ . The dye concentration was determined by using a UV-VIS spectrophotometer UV-2600 (Shimadzu) at a wavelength of 595 nm, using a previously established calibration curve. The pH modification on dye solutions did not alter the chemical structure of the dye (*cf.* ESI, Fig. S2†).<sup>35</sup> To determine the amount of dye adsorbed, eqn (1) was used:

$$q_e = \frac{C_0 - C_e}{m} \times V \quad (1)$$

where  $q_e$  is the equilibrium adsorption capacity (*i.e.* the amount of dye-adsorbed ( $\text{mg g}^{-1}$ ) on the adsorbent at equilibrium),  $C_0$

and  $C_e$  are the initial and equilibrium concentrations of the dye ( $\text{mg L}^{-1}$ ), respectively,  $m$  is the mass of the adsorbent used (mg), and  $V$  is the volume of dye solution (L).

The adsorption kinetic data generally follow one of the two kinetic models, namely the Pseudo First-Order (PFO) or the Pseudo Second-Order (PSO) models, which are described using the following equations, respectively:

$$\frac{dq_t}{dt} = k_1 \times (q_e - q_t) \quad (2)$$

$$\frac{dq_t}{dt} = k_2 \times (q_e - q_t)^2 \quad (3)$$

where  $k_1$  is the PFO constant ( $\text{min}^{-1}$ ) and  $k_2$  is the PSO constant ( $\text{min}^{-1}$ ),  $q_e$  is the amount of sorbent bound to the sorbate at the equilibrium ( $\text{mg g}^{-1}$ ),  $q_t$  is the amount of sorbent bound to the sorbate at a given time ( $\text{mg g}^{-1}$ ), and  $t$  is the time (min).

## Results and discussion

### Keratin-based film characterisation

The FTIR-ATR spectra are shown in Fig. 2, showing the essential absorption bands representative of keratin-based films. The presence of keratin is confirmed by the stretching vibrations of O–H and N–H (Amide A) at 3670–2800  $\text{cm}^{-1}$ , C=O stretching (Amide I) at 1700–1600  $\text{cm}^{-1}$ , N–H bending and C–H stretching (Amide II) at 1590–1470  $\text{cm}^{-1}$ , and amide III (1280–1200  $\text{cm}^{-1}$ ). In general, all keratin films present the same bands, except for the keratin films obtained by adding glycerol as a plasticiser, where a band at 1070–1000  $\text{cm}^{-1}$  is also observed, indicative of the presence of the added alcohol.<sup>36</sup> Regarding the blends, the hydroxyl group broad stretching at 3300  $\text{cm}^{-1}$  and 1650  $\text{cm}^{-1}$  is related to the water absorption and hydroxyl groups present in the cellulose,<sup>37</sup> while the band at 1060  $\text{cm}^{-1}$  is attributed to the C–O asymmetric stretching vibration of the glycosidic ring in cellulose.<sup>38</sup> The bands at 1650  $\text{cm}^{-1}$  and 1560  $\text{cm}^{-1}$  are related to chitin's amide vibrations, assigned to the C=O stretching and N–H bending.<sup>39</sup> Overall, these results reveal that the biopolymers are well blended.

Regarding the thermal behaviour (ESI, Fig. S3†), all keratin-based films presented more than one step of degradation, with the first degradation step, likely related to moisture, occurring at below 100  $^{\circ}\text{C}$ . The second stage corresponds to keratin decomposition for pure keratin films (without adding cellulose or chitin). All keratin film samples (prepared with different ILs, solution pH, keratin concentration, and glycerol added) were stable up to 215  $^{\circ}\text{C}$  and revealed a similar behaviour. The bio-composite blends (with different ratios of keratin–cellulose and keratin–chitin) exhibited similar behaviour and were stable up to 160  $^{\circ}\text{C}$ . The samples were decomposed between 160  $^{\circ}\text{C}$  and 360  $^{\circ}\text{C}$ , with a slow degradation, divided into steps, thus indicating physical interactions, and no chemical interactions, between the biopolymers (the thermal degradation of cellulose and chitin correspond to 335  $^{\circ}\text{C}$  (ref. 40) and 253  $^{\circ}\text{C}$ ,<sup>41</sup> respectively). The starting decomposition at 160  $^{\circ}\text{C}$  can be related to glycerol evaporation (boiling temperature = 182  $^{\circ}\text{C}$ ). In general, the results are within the range of the thermal degradation



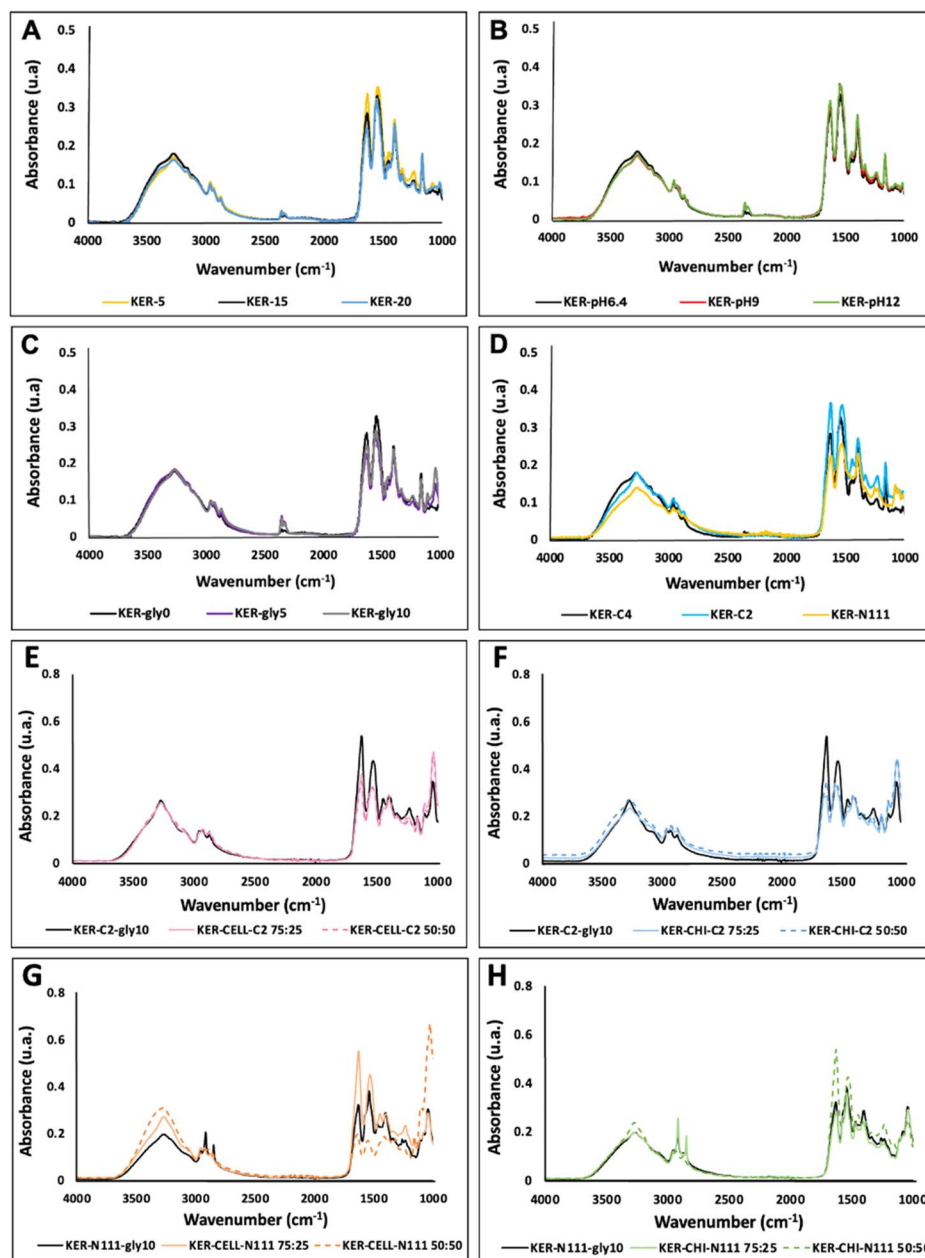


Fig. 2 FTIR spectra of keratin-based film samples processed using different conditions: varying protein concentration (A); pH of the solution (B); addition of glycerol (C); using different acetate-based ILs (D); keratin–cellulose blend films processed by  $[C_2C_1im][C_1CO_2]$  (E); keratin–chitin blend films processed by  $[C_2C_1im][C_1CO_2]$  (F); keratin–cellulose blend films processed by  $[N_{111(2OH)}][C_1CO_2]$  (G); and keratin–chitin blend films processed by  $[N_{111(2OH)}][C_1CO_2]$  (H).

obtained for keratin<sup>6,11,42</sup> and other protein films, such as soy protein films (180 °C)<sup>43</sup> and whey protein films (295 °C).<sup>44</sup>

The wettability of keratin-based films was assessed by measuring the contact angle of ethylene glycol drops on the films (Table 2). The contact angle of all keratin-based films was found to be lower than 90°, confirming their hydrophilic nature due to the presence of hydrogen bond donor and acceptor groups, such as amino, carboxylic and hydroxyl groups. Furthermore, no significant variations in the contact angle were observed across different IL films, ranging from (55 ± 1)° to (60 ± 5)°, meaning that there is no IL residue on the keratin-based

films and that their use in keratin processing does not cause significant differences in keratin properties. Nevertheless, when keratin films were prepared with higher pH, the contact angle value increased from (55 ± 1)° to (84 ± 1)°, indicating that increasing pH can promote a more hydrophobic film. This behaviour is attributed to the alkaline pH, which results in stronger intramolecular electrostatic repulsion and unfolding of proteins, exposing their hydrophobic groups and amino acid residues. Furthermore, the films with glycerol were more hydrophilic, which is due to its plasticiser effect and the presence of additional polar hydroxyl groups. The addition of



10 wt% glycerol decreased the contact angle from  $(55 \pm 1)^\circ$  to  $(47 \pm 5)^\circ$ . The same behaviour was observed by Cerqueira *et al.*,<sup>45</sup> who investigated the influence of glycerol on chitosan films.

The wettability of the keratin–cellulose and keratin–chitin films ranges from  $(47 \pm 2)^\circ$  to  $(63 \pm 3)^\circ$ , supporting their hydrophilic nature. For the keratin–cellulose films, increasing the cellulose content from 25 wt% to 50 wt% resulted in an increase of  $9^\circ$  in the contact angle for films produced with both ILs. This is a direct result of the higher cellulose hydrophobic nature. A contrasting behaviour was observed for keratin–chitin films, with the contact angle decreasing by  $16^\circ$  when chitin addition increased from 25 wt% to 50 wt%. This behaviour can be attributed to the interaction between the biopolymers, leading to a higher exposure of their hydrophilic amino acids. Deng *et al.*,<sup>46</sup> who processed wool keratin–cellulose membranes with different ratios, also obtained hydrophilic biomaterials, with changes in the contact angle from  $61^\circ$  to  $80^\circ$ .<sup>46</sup> To the best of our knowledge, no results regarding keratin–chitin films have yet been reported. Tomihata *et al.*<sup>47</sup> evaluated the contact angle of chitin films and obtained  $69.5^\circ$ , thus confirming the hydrophilicity of chitin films.

Tensile strength refers to the ability of a film to resist tensile stress before breaking, being the results obtained for the investigated keratin-based films summarised in Table 2. The tensile strength of keratin films increased 26 times by increasing the keratin concentration from 5 wt% to 15 wt%, ranging from  $(0.53 \pm 0.04)$  MPa (KER-5) to  $(14 \pm 2)$  MPa (KER-15). No further increase in the tensile strength was observed when increasing the keratin concentration from 15 wt% (KER-15) to 20 wt% (KER-20). Concerning the pH and use of various ILs, no significant differences were observed. The addition of

glycerol as a plasticiser increased the tensile strength of the film 3.5 times, going from  $(14 \pm 2)$  MPa (KER-gly0) to  $(50 \pm 1)$  MPa (KER-gly10). Therefore, among the variables evaluated in this work, the keratin concentration and glycerol addition presented the highest impact on the films' tensile strength. Shahrim *et al.*<sup>48</sup> also observed this glycerol effect while investigating the tensile strength of starch films. The results obtained by the authors revealed an increase in tensile strength of 7% when increasing the glycerol from 5% to 10%,<sup>48</sup> which is lower than the increase observed with the keratin films studied here.

For the blends, the tensile strength of keratin–cellulose films did not present a significant increase when the addition of cellulose increased from 25 wt% to 50 wt%. Furthermore, increases of 1.1 and 1.4 times were observed for the films processed with keratin dissolved using  $[N_{111}(2OH)][C_1CO_2]$  and  $[C_2C_1im][C_1CO_2]$ , respectively.

These results suggest that using  $[C_2C_1im][C_1CO_2]$  for dissolution leads to more resistant films. The maximum tensile strength obtained for the keratin–cellulose blend was  $(30 \pm 3)$  MPa, achieved with KER–CELL–C2 50 : 50. On the other hand, considering blends with chitin, the highest tensile strength of  $66 \pm 1$  MPa was obtained for KER–CHI–C2 50 : 50, demonstrating the benefit of adding chitin due to its more promising mechanical properties.<sup>49</sup>

Ma *et al.*<sup>50</sup> prepared keratin–cellulose films with various ratios and showed that the blends have poor mechanical properties compared to pure cellulose films. According to the authors, the pure cellulose film had a higher tensile strength (44 MPa) than a keratin–cellulose 40 : 60 film (28 MPa).<sup>50</sup> The authors did not report films with higher amounts of keratin; however, these results show that more cellulose could be essential to create a stronger film. Concerning the authors' process, keratin was recovered from wool using urea, sodium dodecyl sulphate, and sodium bisulphite. After protein dialysis, the liquid was cast on a polypropylene mould, dried, and dissolved in formic acid to prepare a keratin solution. Another solution was prepared for cellulose by dissolving the polysaccharide in NMMO solution under heating. On the other hand, to the best of our knowledge, no results have yet been reported for keratin–chitin films. However, looking for pure chitin films, Wu *et al.*<sup>49</sup> obtained a high tensile strength value for their films (320 MPa), confirming chitin's high tensile strength.

The morphological properties of keratin films (ESI, Fig. S4†) were determined using SEM. All keratin films, except KER–pH12 and KER–gly10, present a smooth surface. In KER–pH12, a particular behaviour can be noticed due to the presence of salt (in this case, NaOH, used to adjust the solution pH). In contrast, the roughness in KER–gly10 may be due to the addition of glycerol and solution destabilization during casting and drying. SEM analysis was also performed to illustrate the morphological effects of keratin–blend films, being shown in ESI, Fig. S5.† In general, the films are homogeneous, suggesting an appropriate blending; however, there were some irregularities observed in the blended films, indicating the presence of biopolymer particles on the film's surface, which can be related to possible differences in coagulation for each biopolymer.

Table 2 Contact angle and tensile strength of keratin-based films<sup>a</sup>

Samples	Contact angle ( $^\circ$ )	Tensile strength (MPa)
KER-5	$23 \pm 2$	$0.53 \pm 0.04$
KER-15*	$55 \pm 1$	$14 \pm 2$
KER-20	$62 \pm 1$	$14 \pm 2$
KER–pH6.4*	$55 \pm 1$	$14 \pm 2$
KER–pH9	$86 \pm 2$	$10 \pm 1$
KER–pH12	$84 \pm 1$	$11 \pm 2$
KER–gly0*	$55 \pm 1$	$14 \pm 2$
KER–gly5	$49 \pm 2$	$36 \pm 1$
KER–gly10	$47 \pm 5$	$50 \pm 1$
KER–C4*	$55 \pm 1$	$14 \pm 2$
KER–C2	$58 \pm 5$	$12 \pm 1$
KER–N <sub>111</sub>	$60 \pm 5$	$11 \pm 1$
KER–CELL–C2 75 : 25	$54 \pm 2$	$21 \pm 1$
KER–CELL–C2 50 : 50	$63 \pm 3$	$30 \pm 3$
KER–CHI–C2 75 : 25	$63 \pm 1$	$53 \pm 2$
KER–CHI–C2 50 : 50	$47 \pm 2$	$66 \pm 1$
KER–CELL–N <sub>111</sub> 75 : 25	$54 \pm 3$	$23 \pm 1$
KER–CELL–N <sub>111</sub> 50 : 50	$62 \pm 2$	$26 \pm 3$
KER–CHI–N <sub>111</sub> 75 : 25	$59 \pm 2$	$34 \pm 2$
KER–CHI–N <sub>111</sub> 50 : 50	$48 \pm 2$	$41 \pm 5$

<sup>a</sup> \*KER-15 = KER–pH6.4 = KER–gly0 = KER–C4.



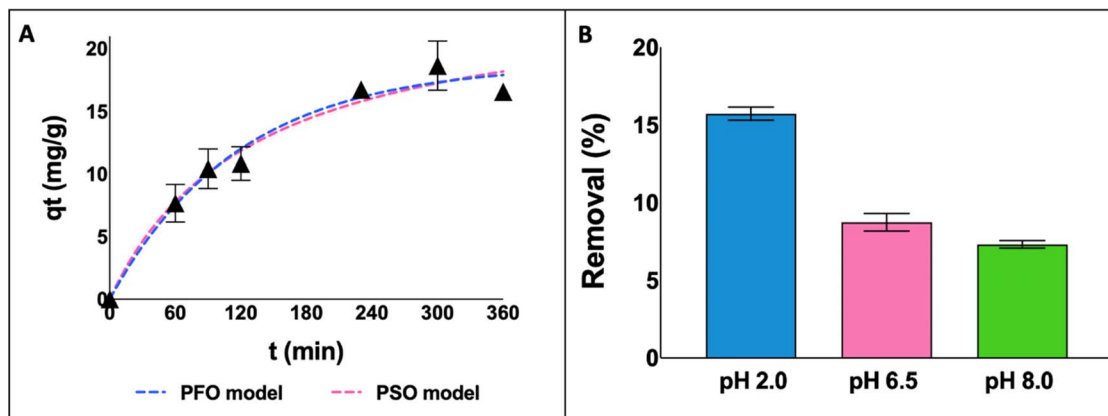


Fig. 3 Adsorption kinetics curves for the KER-CHI-C2 film as a function of time (A) and the effect of pH on the adsorption of RB4 by KER-CHI-C2 (B).

### Dye adsorption using keratin-based films

With the aim of preparing stronger keratin-based films for dye adsorption studies, the films processed with  $[C_2C_1im][C_1CO_2]$  were selected due to their superior mechanical properties, specifically tensile strength (see Table 1). Keratin (KER-gly10), keratin-cellulose (KER-CEL-C2 50:50), and keratin-chitin films (KER-CHI-C2 50:50) were applied to investigate the effects of the biopolymers on dye adsorption. Different adsorption experiments were carried out by varying the RB4 initial concentration, pH, time and adsorbent type.

First, aiming to understand the adsorption process and identify the contact time necessary to achieve the equilibrium stage, adsorption kinetic experiments were performed for the KER-CHI-C2 film at pH 2.0, from 0 to 360 min (Fig. 3A). Then, the pH effect (from 2.0 to 8.0) was evaluated for the same adsorbent at 300 min (Fig. 3B). The respective parameters from the fitting of adsorption kinetic experimental data with PFO and PSO models are given in Table 3.

According to the adsorption kinetic curves (Fig. 3A), the equilibrium stage was achieved between 240 and 360 min and maintained for 300 min in the next experiments. Looking at Table 3, despite both models presenting a good fit to the experimental data, PFO presented the best fit ( $R^2 = 0.96$ ), suggesting that the adsorption process occurs on localised sites and does not involve interactions with the adsorbed molecules.<sup>51</sup>

By decreasing the pH from 8.0 to 2.0 (Fig. 3B), a significant increase in RB4 removal is obtained for KER-CHI-C2, moving from 7.3% to 15.7%. This behaviour can be explained by the pH value at zero potential point of the keratin-based films (4–5), which means

Table 3 Adsorption parameters obtained from the fitting of adsorption kinetic experimental data with PFO and PSO models alongside the respective correlation coefficients

PFO model			PSO model		
$q_e$ (mg g <sup>-1</sup> )	$k_1$ (min <sup>-1</sup> )	$R^2$	$q_e$ (mg g <sup>-1</sup> )	$k_2$ (min <sup>-1</sup> )	$R^2$
18.82	0.0084	0.96	24.86	0.0003	0.95

that under acidic conditions the adsorbent is protonated, promoting electrostatic interactions with the dye. RB4 has two sulfonate groups and a primary amino group, with  $pK_a$  values of 0.8 and 7.0, respectively. These groups can be easily dissociated; thus, the dye molecule has negative and positive charges under the working experimental conditions. The diverse keratin functional groups (e.g.  $-NH_2$ ,  $-COOH$ ,  $-SH$ , and  $-OH$ ) make it a promising adsorbent.<sup>52</sup> Accordingly, the adsorption mechanism of keratin-based films for RB4 dye is mainly ruled by electrostatic attractions (between the  $-OH$  group of keratin and the sulfonate ( $-SO_3^-$ ) group on the RB4 structure) and hydrogen bonding interactions (between the  $-OH$  group of keratin and the nitrogen group on the RB4 structure).<sup>24,53</sup>

### Adsorption isotherms

Adsorption isotherms were determined to investigate the relationship between the adsorbent and the dye adsorbed under equilibrium conditions. The two models most widely used to represent equilibrium isotherms for adsorbent materials were applied: the Langmuir and Freundlich models.<sup>54</sup>

Langmuir (eqn (4)) is a model based on homogeneous monolayer adsorption on a homogeneous surface, while Freundlich (eqn (5)) is based on heterogeneous adsorption.<sup>54</sup>

$$q_e = q_{\max} \times \frac{k_L \times C_e}{1 + k_L \times C_e} \quad (4)$$

where  $q_{\max}$  is the maximum adsorption capacity of the adsorbent (mg g<sup>-1</sup>),  $k_L$  is the Langmuir constant (L mg<sup>-1</sup>),  $C_e$  corresponds to the dye concentration in the solution (mg L<sup>-1</sup>), and  $q_e$  is the adsorption capacity of the adsorbent (mg g<sup>-1</sup>), at the equilibrium.

$$q_e = k_f \times C_e^{\frac{1}{n}} \quad (5)$$

where  $k_f$  is the Freundlich constant related to the adsorption capacity (mg g<sup>-1</sup>) (L mg<sup>-1</sup>)<sup>1/n</sup> and  $n$  is an empirical parameter related to adsorption intensity.

Fig. 4 shows the Langmuir and Freundlich's fittings for all keratin-based films at pH 2.0. The parameter values of the



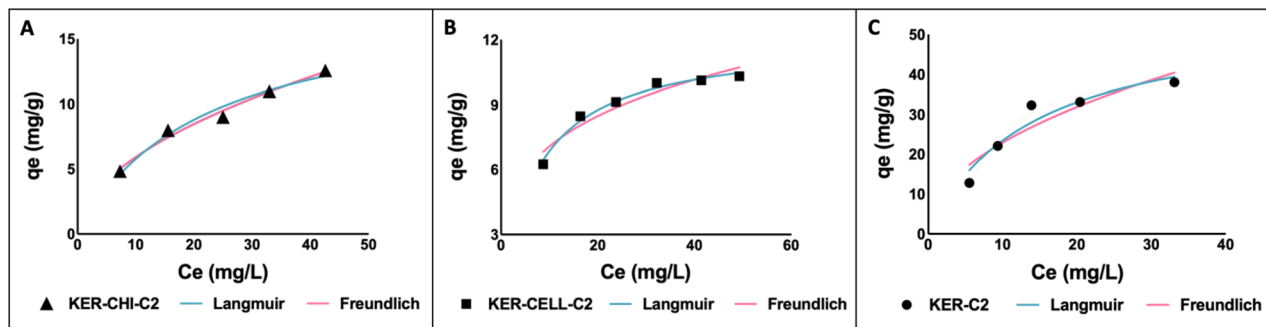


Fig. 4 Experimental adsorption isotherms of RB4 at pH 2.0 using different keratin-based films: KER-CHI-C2 (A); KER-CELL-C2 (B); and KER-C2 film (C).

Table 4 Parameters obtained for RB4 adsorption using the Langmuir and Freundlich models

Samples	Model	Parameter	Value	$R^2$
KER-CHI-C2	Langmuir	$q_{\max}$ ( $\text{mg g}^{-1}$ )	18.35	0.97
		$k_L$ ( $\text{L mg}^{-1}$ )	0.05	
	Freundlich	$k_f$ ( $(\text{mg g}^{-1}) (\text{L mg}^{-1})^{1/n}$ )	1.81	0.98
		$n$	1.95	
KER-CELL-C2	Langmuir	$q_{\max}$ ( $\text{mg g}^{-1}$ )	12.09	0.99
		$k_L$ ( $\text{L mg}^{-1}$ )	0.13	
	Freundlich	$k_f$ ( $(\text{mg g}^{-1}) (\text{L mg}^{-1})^{1/n}$ )	3.89	0.92
		$n$	3.85	
KER-C2	Langmuir	$q_{\max}$ ( $\text{mg g}^{-1}$ )	55.71	0.92
		$k_L$ ( $\text{L mg}^{-1}$ )	0.07	
	Freundlich	$k_f$ ( $(\text{mg g}^{-1}) (\text{L mg}^{-1})^{1/n}$ )	7.76	0.86
		$n$	2.1	

Langmuir and Freundlich isotherms and the related correlation coefficients ( $R^2$ ) are reported in Table 4. Both models presented satisfactory fittings; however, the Langmuir model yielded better fitting, showing  $R^2$  values higher than 0.92. This trend indicates that the dye adsorption on the adsorbent occurs in a homogeneous surface with monolayer sorption<sup>54</sup> and that the adsorption is of chemical nature.<sup>55</sup> These results are in accordance with the previously discussed results, where it was shown the relevance of the pH and of electrostatic interactions between the dye and the polymers. Furthermore, the maximum adsorption capacity obtained in this work ( $55.71 \text{ mg g}^{-1}$ ) for KER-C2 film confirms that keratin is a fibrous protein with diverse functional groups (e.g. hydrophobic and hydrophilic amino acids and carboxyl groups),<sup>14,23,24</sup> acting as an efficient adsorbent for RB4.

According to the results depicted in Fig. 4, the higher adsorption capacity ( $55.71 \text{ mg g}^{-1}$ ) obtained in this work for RB4 dye is comparable to other adsorbents reported in the literature, such as chitosan-glutaraldehyde beads ( $1.8 \text{ mg g}^{-1}$ )<sup>56</sup> and cellulose-epichlorohydrin polymers ( $69.8 \text{ mg g}^{-1}$ ).<sup>57</sup>

## Conclusions

In this study, a sustainable approach for keratin recovery from chicken feather waste was employed, allowing the preparation

of keratin-based films, either in their pure form or blended with chitin and cellulose. Various processing conditions were investigated to improve the film's mechanical properties. Our findings confirmed that keratin-based films' mechanical properties, particularly the tensile strength, can be improved, principally by increasing the protein concentration and by adding glycerol or with keratin-chitin blends.

To evaluate the use of keratin-based films as adsorbent materials, RB4 adsorption tests were performed under different conditions. RB4, a toxic and widely used dye in the textile industry, was efficiently removed by decreasing the pH. Moreover, the Langmuir isotherm better described the obtained experimental results, indicating that the RB4 adsorption occurs in a monolayer and is of a chemical nature. Overall, the maximum adsorption capacity obtained in this work ( $55.71 \text{ mg g}^{-1}$ ) for the KER-C2 film confirms the efficiency of keratin as an adsorbent due to its functional groups (e.g.  $-\text{NH}_2$ ,  $-\text{COOH}$ ,  $-\text{SH}$ , and  $-\text{OH}$ ). As future steps, evaluating the recycling and reuse of keratin-based films (e.g. by desorption) is crucial to attend to a more sustainable process.

Overall, this work provides new perspectives for chicken feather waste valorisation, recovering keratin and processing keratin-based films (pure or blended with cellulose or chitin) that can be successfully used as adsorption biomaterials. This attempt shows the promise of keratin-based films for dye removal, addressing the possibility of chicken feathers' economic valorisation and overcoming the challenging removal of water-soluble dyes using a renewable, sustainable, and low-cost biomaterial. Notably, our investigation also marks the first reported results on the development of keratin-chitin films, proving that chitin can be used instead of chitosan, and whose industrial production still produces high amounts of liquid effluents from the deacetylation of chitin with concentrated NaOH.<sup>58</sup>

## Data availability

The authors of the manuscript "Ionic-liquid-processed keratin-based biocomposite films with cellulose and chitin for sustainable dye removal" confirm that the data supporting the findings of this study are available within the article and/or its ESI.†





## Author contributions

Conceptualisation, C. P., J. H., H. P., P. Y. S. N., J. A. P. and M. G. F.; methodology, C. P. and P. Y. S. N.; writing – original draft preparation, C. P.; writing – review and editing, J. H., H. P., P. Y. S. N., J. A. P. C. and M. G. F.; supervision, J. H., H. P., and M. G. F.; funding acquisition, J. H. and M. G. F.; project administration, J. H. and M. G. F. All authors listed have made a substantial, direct, and intellectual contribution to the work and agreed to the published version of the manuscript.

## Conflicts of interest

There are no conflicts to declare.

## Acknowledgements

This work was developed within the scope of the project CICECO-Aveiro Institute of Materials, UIDB/50011/2020 (DOI 10.54499/UIDB/50011/2020), UIDP/50011/2020 (DOI 10.54499/UIDP/50011/2020) & LA/P/0006/2020 (DOI 10.54499/LA/P/0006/2020), financed by national funds through the FCT/MCTES (PIDDAC). C. Polesca acknowledges FCT – Fundação para a Ciência e a Tecnologia for the PhD grant with the reference UI/BD/151282/2021 (DOI 10.54499/UI/BD/151282/2021). This work was supported by national funds through FCT/MCTES (PIDDAC): LSRE-LCM, UIDB/50020/2020 (DOI: 10.54499/UIDB/50020/2020) and UIDP/50020/2020 (DOI: 10.54499/UIDP/50020/2020); and ALiCE, LA/P/0045/2020 (DOI: 10.54499/LA/P/0045/2020). J. H. and P. Y. S. N. were supported by the UKRI Supergen Bioenergy Impact Hub.

## Notes and references

- 1 Y. Y. Khaw, C. Y. Chee, S. N. Gan, R. Singh, N. N. N. Ghazali and N. S. Liu, *J. Appl. Polym. Sci.*, 2019, **136**, 47642–47651.
- 2 M. Peydayesh, M. Bagnani, W. L. Soon and R. Mezzenga, *Chem. Rev.*, 2023, **123**, 2112–2154.
- 3 Z. Wang, X. Yan, C. Cong, G. Xing, Z. Wang and J. Wang, *ACS Sustain. Chem. Eng.*, 2023, **11**, 6032–6042.
- 4 E. M. Nuutinen, T. Virtanen, R. Lantto, M. Vähä-Nissi and A. S. Jääskeläinen, *RSC Adv.*, 2021, **11**, 27512–27522.
- 5 X. Liu, Y. Nie, Y. Liu, S. Zhang and A. L. Skov, *ACS Sustain. Chem. Eng.*, 2018, **6**, 17314–17322.
- 6 A. Idris, R. Vijayaraghavan, U. A. Rana, D. Fredericks, A. F. Patti and D. R. MacFarlane, *Green Chem.*, 2013, **15**, 525–534.
- 7 A. Idris, R. Vijayaraghavan, U. A. Rana, A. F. Patti and D. R. MacFarlane, *Green Chem.*, 2014, **16**, 2857–2864.
- 8 Y. J. Yang, D. Ganbat, P. Aramwit, A. Bucciarelli, J. Chen, C. Migliaresi and A. Motta, *EXPRESS Polym. Lett.*, 2019, **13**, 97–108.
- 9 X. Liu, Y. Nie, X. Meng, Z. Zhang, X. Zhang and S. Zhang, *RSC Adv.*, 2017, **7**, 1981–1988.
- 10 Z. Zhang, Y. Nie, Q. Zhang, X. Liu, W. Tu, X. Zhang and S. Zhang, *ACS Sustain. Chem. Eng.*, 2017, **5**, 2614–2622.
- 11 C. Polesca, H. Passos, B. M. Neves, J. A. P. Coutinho and M. G. Freire, *Green Chem.*, 2023, **25**, 1424–1434.
- 12 C. Polesca, H. Passos, J. A. P. Coutinho and M. G. Freire, *Curr. Opin. Green Sustainable Chem.*, 2022, 100675.
- 13 C. Polesca, A. Al Ghatta, H. Passos, J. A. P. Coutinho, J. P. Hallett and M. G. Freire, *Green Chem.*, 2023, **25**, 3995–4003.
- 14 T. Posati, A. Listwan, G. Sotgiu, A. Torreggiani, R. Zamboni and A. Aluigi, *Front. Bioeng. Biotechnol.*, 2020, **8**, 68.
- 15 K. Song, X. Qian, X. Zhu, X. Li and X. Hong, *J. Colloid Interface Sci.*, 2020, **579**, 28–36.
- 16 P. Gao, K. Li, Z. Liu, B. Liu, C. Ma, G. Xue and M. Zhou, *Water, Air, Soil Pollut.*, 2014, **225**, 1946.
- 17 Safety Data Sheet for Reactive Blue 4, Sigma-Aldrich Safety Data Sheet.
- 18 T. Yuan, S. Zhang, Y. Chen, R. Zhang, L. Chen, X. Ruan, S. Zhang and F. Zhang, *Front. Microbiol.*, 2021, **12**, 644679.
- 19 W. J. Epolito, Y. H. Lee, L. A. Bottomley and S. G. Pavlostathis, *Dyes Pigm.*, 2005, **67**, 35–46.
- 20 N. A. Abd El-Ghany, M. H. A. Elella, H. M. Abdallah, M. S. Mostafa and M. Samy, *J. Polym. Environ.*, 2023, 2792–2825.
- 21 A. G. Varghese, S. A. Paul and M. S. Latha, *Environ. Chem. Lett.*, 2019, **17**, 867–877.
- 22 S. Rastogi and B. Kandasubramanian, *Environ. Sci. Pollut. Res.*, 2020, **27**, 210–237.
- 23 P. Pradhan and A. Bajpai, *Mater. Today: Proc.*, 2020, **29**, 1204–1212.
- 24 W. Zhu, X. Qian, H. Yu, X. Li and K. Song, *Environ. Sci. Pollut. Res.*, 2020, **27**, 41577–41584.
- 25 S. Wei, X. Hou, L. Liu, Y. Tian, W. Li and H. Xu, *J. Nat. Fibers*, 2022, **20**, 2157362.
- 26 I. Zahara, M. Arshad, M. A. Naeth, T. Siddique and A. Ullah, *Chemosphere*, 2021, **273**, 128545.
- 27 X. Mi, H. Xu and Y. Yang, *Colloids Surf., B*, 2019, **177**, 33–40.
- 28 B. Ocak, *Biomass Convers. Biorefin.*, 2022, **14**, 12397–12410.
- 29 B. Blessing, C. Trout, A. Morales, K. Rybacki, S. A. Love, G. Lamoureux, S. M. O'malley, X. Hu and D. Salas-De la Cruz, *Int. J. Mol. Sci.*, 2020, **21**, 1–23.
- 30 B. Baghaei and M. Skrifvars, *Molecules*, 2020, **25**, 2836.
- 31 P. Sirajudheen, N. C. Poovathumkuzhi, S. Vigneshwaran, B. M. Chelaveetil and S. Meenakshi, *Carbohydr. Polym.*, 2021, **273**, 118604.
- 32 J. Cui, Z. Yu and D. Lau, *Int. J. Mol. Sci.*, 2016, **17**, 1–13.
- 33 B. Y. Alashwal, M. Saad Bala, A. Gupta, S. Sharma and P. Mishra, *J. King Saud Univ., Sci.*, 2020, **32**, 853–857.
- 34 N. Muhammad, M. I. Hossain, Z. Man, M. El-Harbawi, M. A. Bustam, Y. A. Noaman, N. B. Mohamed Alitheen, M. K. Ng, G. Hefter and C. Y. Yin, *J. Chem. Eng. Data*, 2012, **57**, 2191–2196.
- 35 *MarvinSketch 21.14*, ChemAxo, 2021, <https://chemaxon.com/>.
- 36 N. Striugas, R. Skvorčinskienė, R. Paulauskas, K. Zakarauskas and L. Vorotinskienė, *Fuel*, 2017, **204**, 227–235.
- 37 D. C. M. Ribeiro, R. C. Rebelo, F. De Bon, J. F. J. Coelho and A. C. Serra, *Polymers*, 2021, **13**, 1767–1782.



- 38 F. W. Low, N. A. Samsudin, Y. Yusoff, X. Y. Tan, C. W. Lai, N. Amin and S. K. Tiong, *Thermochim. Acta*, 2020, **684**, 178484–178492.
- 39 C. Gonçalves, S. S. Silva, J. M. Gomes, I. M. Oliveira, R. F. Canadas, F. R. Maia, H. Radhouani, R. L. Reis and J. M. Oliveira, *ACS Sustain. Chem. Eng.*, 2020, **8**, 3986–3994.
- 40 K. Rybacki, S. A. Love, B. Blessing, A. Morales, E. McDermott, K. Cai, X. Hu and D. Salas-De La Cruz, *ACS Mater. Au*, 2022, **2**, 21–32.
- 41 C. King, J. L. Shamshina, G. Gurau, P. Berton, N. F. A. F. Khan and R. D. Rogers, *Green Chem.*, 2017, **19**, 117–126.
- 42 S. Alahyaribeik and A. Ullah, *Int. J. Biol. Macromol.*, 2020, **148**, 449–456.
- 43 P. Guerrero, A. Retegi, N. Gabilondo and K. De La Caba, *J. Food Eng.*, 2010, **100**, 145–151.
- 44 P. L. M. Barreto, A. T. N. Pires and V. Soldi, *Polym. Degrad. Stab.*, 2023, **79**, 147–152.
- 45 M. A. Cerqueira, B. W. S. Souza, J. A. Teixeira and A. A. Vicente, *Food Hydrocolloids*, 2012, **27**, 175–184.
- 46 L. Deng, W. Yue, L. Zhang, Y. Guo, H. Xie, Q. Zheng, G. Zou and P. Chen, *ACS Sustain. Chem. Eng.*, 2022, **10**, 2158–2168.
- 47 K. Tomihata and Y. Ikada, *Biomaterials*, 1997, **18**, 567–575.
- 48 N. A. Shahrim, N. Sarifuddin, H. H. M. Zaki and A. Z. A. Azhar, *Malaysian Journal of Analytical Sciences*, 2018, **22**, 892–898.
- 49 Q. Wu, E. Jungstedt, M. Šoltésová, N. E. Mushi and L. A. Berglund, *Nanoscale*, 2019, **11**, 11001–11011.
- 50 Y.-Y. Ma, R.-R. Qi, S.-Y. Jia and Z.-H. Wang, *Int. J. Biol. Macromol.*, 2016, **89**, 614–621.
- 51 L. Largette and R. Pasquier, *Chem. Eng. Res. Des.*, 2016, **109**, 495–504.
- 52 K. Oussadi, S. Al-Farraj, B. Benabdallah, A. Benettayeb, B. Haddou and M. Sillanpaa, *Biomass Convers. Biorefin.*, 2024, DOI: [10.1007/s13399-024-05851-4](https://doi.org/10.1007/s13399-024-05851-4).
- 53 P. Praipipat, P. Ngamsurach, A. Thanyahan, A. Sakda and J. Nitayarat, *Ind. Crops Prod.*, 2022, **7**, 41744–41758.
- 54 A. Paton-Carrero, P. Sanchez, L. Sánchez-Silva and A. Romero, *Mater. Today Commun.*, 2021, 103033.
- 55 G. L. Dotto, M. Luiza, G. Vieira, J. Oliveira Gonçalves, L. Antônio and A. Pinto, *Quim. Nova*, 2011, **34**, 1193–1199.
- 56 J. Galan, J. Trilleras, P. A. Zapata, V. A. Arana and C. D. Grande-Tovar, *Life*, 2021, **11**, 1–20.
- 57 Y. Zhai, H. Qu, Z. Li, B. Zhang, J. Cheng and J. Zhang, *Trans. Tianjin Univ.*, 2021, **27**, 77–86.
- 58 A. Riofrio, T. Alcivar and H. Baykara, *ACS Omega*, 2021, **6**, 23038–23051.

